Powder XRD analysis and catalysis characterization of ultra-small gold nanoparticles deposited on titania-modified SBA-15

Wenfu Yan [a], Valeri Petkov [b,*], Shannon M. Mahurin [a],
Steven H. Overbury [a], Sheng Dai [a,*]

[a] Chemical Sciences Division, Oak Ridge National Laboratory, Oak Ridge, TN 37831-6201, United States
[b] Department of Physics, 203 Dow Science, Central Michigan University, Mt. Pleasant, MI 48859, United States

Abstract

Ultra-small gold nanoparticles (0.8–1 nm) are successfully deposited on titania-modified SBA-15 via a deposition–precipitation method. A comparison of experimental X-ray diffraction (XRD) patterns with theoretical ones shows that gold exists as Au^{3+} and Au^0 in the as-synthesized and reduced catalyst, respectively. The XRD analyses also suggest that Au nanoparticles are more developed along the $\langle 1 1 1 \rangle$ direction forming a raft-type structure. Z-contrast transmission electron microscopy analyses indicate that the ultra-small gold nanoparticles are uniformly dispersed on the surface of the substrate. The material is found to possess high catalytic activity for low-temperature CO oxidation.

© 2005 Published by Elsevier B.V.

1. Introduction

Supported gold nanoparticles have been found to be catalytically active for a number of different reactions of both industrial and environmental importance [1–11]. Traditionally, gold nanoparticles are obtained by an impregnation method. This method, however, is only capable of yielding particles of size larger than 30 nm. The constant search for methods delivering smaller and catalytically more active nanoparticles has resulted in the development of several novel physical and chemical preparation approaches. Rousset and co-workers [12] reported a laser vaporization deposition of metallic gold clusters onto high surface area oxides such as γ-Al_2O_3, ZrO_2, and TiO_2. The nanoparticles show a narrow distribution of sizes centered around 3 nm. Scurrell and co-workers [13] reported an in situ reduction of a gold salt ($HAuCl_4$) on a TiO_2 support resulting in fairly uniform gold nanoparticles of mean diameter <5 nm. Iwasawa and co-workers [14,15] used wet as-precipitated metal hydroxides and gold phosphine complexes as precursors for the oxide support and gold particles, respectively, followed by a calcination process. The mean size of the particles obtained by this procedure was reported to be from 2.6 to 9.3 nm. Baiker and co-workers [16] developed a method to "design" the supported Au particles via "size-controlled" gold colloids resulting in particles with a mean size of 2 nm. The gold colloids were obtained by reduction of chloroauric acid with tetrakis(hydroxymethyl) phosphonium chloride in an alkaline solution and were adsorbed on TiO_2 and ZrO_2 supports. Haruta and co-workers [17] developed several approaches to deposit gold nanoparticles on various types of metal oxides including co-precipitation [3], co-sputtering, deposition–precipitation (DP) [18], and gas-phase grafting (GG) [19,20]. These methods can yield particles with mean diameters in the range of

---

* Corresponding authors. Tel.: +1 989 774 3395; fax: +1 989 774 2697 (V. Petkov).

  E-mail addresses: petkov@phy.cmich.edu (V. Petkov), dais@ornl.gov (S. Dai).

55 2–10 nm [21]. With the DP method, it is possible to ob-
56 tain gold particles with a size of 2–3 nm.
57   The surface sol–gel method (SSP) was originally
58 developed by Kunitake and co-workers [22–27] for
59 layer-by-layer deposition on planar substrates. This no-
60 vel technology enables molecular-scale control of film
61 thickness over a large 2D substrate area and can be
62 viewed as a solution-based technique for atomic layer
63 deposition (ALD) synthesis [25–27]. Compared with
64 conventional deposition methods, the surface sol–gel
65 technique offers the advantage of producing ultra-thin
66 conformal films, with control of the thickness and
67 composition of the films at the atomic level. The SSP
68 technique consists of two steps: (i) non-aqueous conden-
69 sation of metal–alkoxide precursor molecules with
70 surface hydroxyl groups; (ii) aqueous hydrolysis of the
71 adsorbed metal–alkoxide species to regenerate surface
72 hydroxyls.
73   We have recently reported the formation of ultra-
74 small gold nanoparticles (0.8–1 nm) on the surface of
75 mesoporous silica of SBA-15 uniformly covered with
76 one atomic layer TiO_2 through a surface sol–gel process
77 [28]. The resulting material exhibited high catalytic
78 activities for CO oxidation. The aim of the current work
79 is to analyze the size and structure of gold nanoparticles
80 via powder XRD in correlation with Z-contrast trans-
81 mission electron microscopy (TEM) and CO oxidation
82 catalytic activity tests.

2. Experimental

84   The mesoporous material used in this investigation is
85 SBA-15. The procedure for surface sol–gel process on
86 SBA-15 has been described before [28]. Briefly, 0.8 mL
87 of titanium (IV) butoxide (Aldrich. 97%), 10 mL of
88 anhydrous toluene (Aldrich, 99.8%), and 10 mL of
89 anhydrous methanol (Aldrich, 99.8%) were transferred
90 into a bottle containing 1 g of SBA-15. The resulting
91 solution was vigorously stirred for 3 h at room temper-
92 ature. The product was washed several times with etha-
93 nol and de-ionized (DI) water and dried at 80 °C
94 overnight. Gold deposition was carried out according
95 to the method of Haruta and coworkers [18]. First, 3.0
96 g of hydrogen tetrachloroaurate (III) trihydrate (HAu-
97 $Cl_4 \cdot 3H_2O$, 99.9+%, Aldrich) was dissolved into
98 500 mL de-ionized water to form the gold precursor
99 solution. Typically, the pH value of the pre-weighed
100 gold precursor solution (20 mL) was adjusted to about
101 10 with vigorous stirring using a solution of 1.0 M
102 KOH at room temperature. This high pH value allows
103 us to control the deposition species and concentration
104 [29]. The solution was then heated at 70 °C in a water
105 bath and the surface-modified SBA-15 (0.4 g) was added
106 while stirring. The resulting cloudy solution was contin-
107 ually stirred for 2 h. The precipitates were separated by

108 centrifugation and washed three times with de-ionized
109 water. The resulting product was dried at 40 °C
110 overnight.
111   TEM and Z-contrast microscopy were carried out on
112 a Hitachi HD-2000 STEM operated at 200 kV. Powder
113 X-ray diffraction (XRD) data were collected on a Philips
114 X'Pert diffractometer using Cu Kα radiation
115 ($\lambda = 1.5418$ Å). Theoretical diffraction patterns of Au
116 and Au_2O_3 were calculated using the literature data
117 for the corresponding crystal structures. To simulate
118 the effect of nanocrystallinity, the Bragg intensities in
119 the theoretical diffraction patterns were convoluted with
120 Gaussians having full widths at half maximum
121 (FWHM) of several degrees. The FWHMs were allowed
122 to vary with the diffraction angle according to the equa-
123 tion of Cagliotti et al. [30]. The calculations were per-
124 formed using the program PowderCell [31]. The CO
125 oxidation reaction was carried out with an AMI 200
126 (Altamira Instruments).

3. Results and discussion

128   Experimental powder diffraction spectra for pristine
129 titania-modified SBA-15 (denoted as Ti-SBA-15) and
130 gold loaded Ti-SBA-15 are shown in Fig. 1. As can be
131 seen in the figure, the diffraction pattern of titania-mod-
132 ified mesoporous SBA-15 is typical for a highly disor-
133 dered material. It shows a broad diffraction peak
134 positioned at a Bragg angle (2θ) of 25°, followed by
135 slightly visible oscillations at higher angles. The diffrac-
136 tion pattern of the Au loaded sample shows the same
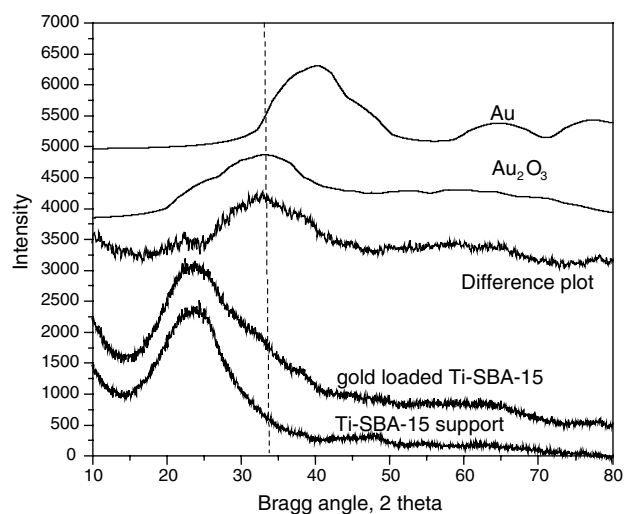
Fig. 1. Experimental powder diffraction spectra for pristine (support) and gold loaded titania-modified SBA-15. The difference between the two experimental spectra is given in the middle. Calculated diffraction spectra for nanocrystalline Au and Au_2O_3 are given in the upper part. The broken line running through the strongest Bragg peak of Au_2O_3 is a guide to the eye.

broad peak with an extra hump on the high-angle side. The difference plot between the patterns of the pristine sample and the Au loaded sample (see Fig. 1) reveals that the hump is indeed a well developed peak which may only be attributed to the deposited Au nanoparticles. To identify the phase state of the nanoparticles we computed diffraction spectra for nanocrystalline Au and Au_2O_3 using the literature data [32,33] for the corresponding crystal structures. The theoretical patterns are also shown in Fig. 1. A comparison between the theoretical data and the difference pattern in Fig. 1 indicates that the latter may not be due to metallic Au. The main peak and the overall profile of the difference data closely resemble the theoretical diffraction pattern of Au_2O_3 suggesting that, as prepared, the Au loaded sample contains Au^{3+} species forming a Au_2O_3 phase. This may not be a surprise since Au_2O_3 is more stable than metallic gold up to 410 K [34]. As can be seen in Fig. 2, the diffraction pattern of the hydrogen reduced sample shows the main peak of the mesoporous support and a new broad feature centered at approximately 40°. A few sharp, but low intensity Bragg peaks are seen as well (follow the broken lines in Fig. 2). The difference plot between the patterns of the pristine and the reduced sample reveals the new diffraction features in more detail. In particular, it shows that the broad feature at 40°, is indeed a highly asymmetric peak having a pronounced high-angle shoulder. The plot resembles the combined profiles of the (111)/(200) pair of Bragg peaks seen in the theoretical diffraction pattern of metallic gold (see Fig. 2). The resemblance suggests that, upon reduction in hydrogen atmosphere, Au^{3+} gold has been

reduced to metallic gold (Au^{0+}) having the usual fcc structure. The difference plot in Fig. 2 also shows the presence of other diffraction peaks of metallic gold such as (220). That peak, while sharp, is quite underdeveloped when compared to the prominent one at 40°. This result suggests that Au nanoparticles are very likely to be more developed along ⟨111⟩ direction forming a raft-type structure.

To estimate the average size, L, of the nanoparticles in the studied samples we employed Sherrer's equation [35]

$$L = \frac{k\lambda}{\beta \cos(\theta)},$$

where $k = 0.94$, λ is the wavelength of the radiation used, β is the full width at half maximum of the peak in radians and θ is the Bragg angle. The equation was applied to the major peaks in the corresponding difference powder diffraction patterns shown in Figs. 1 and 2. The average size of the nanoparticles in the as-synthesized sample was determined to be 0.8(1) nm, and that of the nanoparticles in the sample reduced in H_2 atmosphere at 150 °C was 0.9(1) nm. These estimates are in agreement with our previous TEM experiments showing nanoparticles with size in the range 0.8–1.0 nm [28].

Fig. 3 shows a Z-contrast TEM image of the gold loaded sample. The tiny, highly uniform bright spots (0.8–1.0 nm diameter) along the mesopore channels in Fig. 3 correspond to the gold nanoparticles. The large bright area is likely to originate from bigger gold particles or clusters of ultra-small gold nanoparticles. TEM images of different areas of the sample do not show such bright areas suggesting that the latter are indeed of a very low population. In general, the Z-contrast TEM imaging provides a direct proof for the presence of metallic gold nanoparticles within the channels of
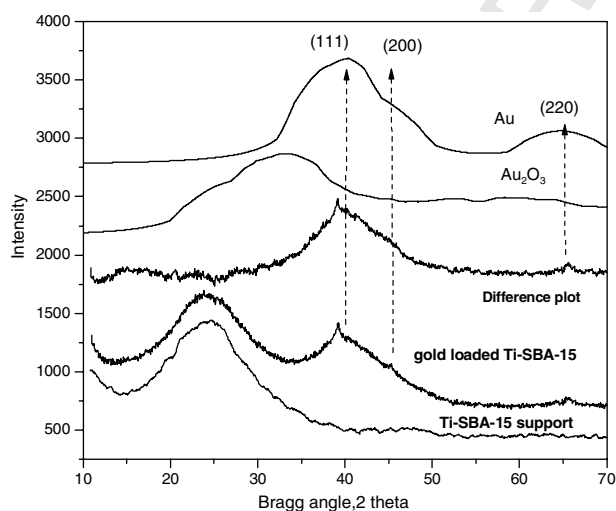
Fig. 2. Experimental powder diffraction spectra for pristine (support) and gold loaded titania-modified SBA-15 reduced in H_2 atmosphere. The difference between the two experimental spectra is given in the middle. Calculated diffraction spectra for nanocrystalline Au and Au_2O_3 are given in the upper part. First few Bragg peaks of Au are marked with arrows.
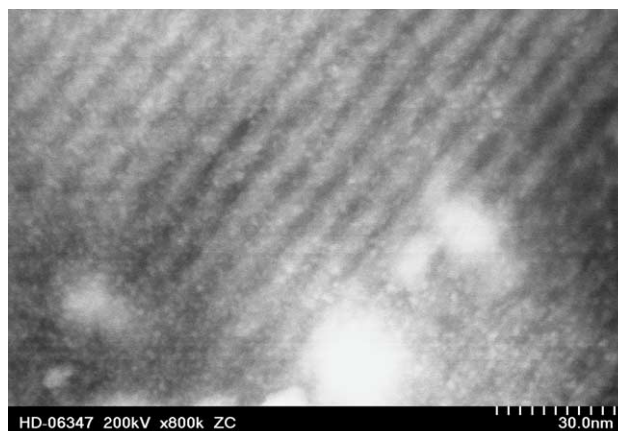
Fig. 3. Z-contrast TEM image of ultra-small gold nanoparticles on ordered mesoporous SBA-15. The bright spots (0.8–1.0 nm) correspond to gold nanoparticles. The large bright area is likely to come from bigger gold particles or clusters of ultra-small gold nanoparticles.

Ti-SBA-15. The key point with high annular dark-field imaging is that the intensity of the Rutherford scattered beams is directly proportional to Z^2, where Z is the atomic number of the scattering element. Thus, heavy atoms (such as gold) stand out very clearly on a light background of silicon and oxygen. The energy-dispersive X-ray (EDX) spectroscopy analysis of the composition of the area shown in Fig. 3 is consistent with the presence of Au and Ti. As our studies show, the deposition of gold on titania-modified mesoporous silica SBA-15 by the DP method results in almost uniform population of ultra-small gold nanoparticles indicating the importance of TiO_2 surfaces for the immobilization and stabilization of gold deposits.

The CO oxidation reaction was carried out with an AMI 200 (Altamira Instruments). Typically, 50 mg of Au-TiO_2 catalyst was packed into a 4 mm ID quartz U-tube and supported by quartz wool. Sample treatments were carried out on the same instrument using pre-mixed 8% O_2–He for oxidation. During the reaction a gas stream of 1% CO balanced with dry air (<4 ppm water) was flowed at ambient pressure through the catalyst at a rate adjusted from sample to sample to maintain a constant space velocity of 44.400 ml/(h g catalyst) or about 37 cm³/min. Gas exiting the reactor was analyzed with Buck Scientific 910 gas chromatograph equipped with dual molecular sieve/porous polymer column (Alltech CTR1) and a thermal conductivity detector. The reaction temperature was varied with an oven or by immersing the U-tube in a dewar of ice water or of cooled acetone which slowly warmed for approximately 10–20 h during the measurement. Catalytic activities comparison between the gold deposited on titania-modified SBA-15 and those on Degussa P-25 sample were performed under above conditions. Comparably high activities (i.e., T_{50}, the temperature which 50% CO conversion achieved, is about $-40\,^{\circ}\text{C}$ were found for both Au catalysts on untreated support. For the as-synthesized catalyst, the value of T_{50} is as low as $-33\,^{\circ}\text{C}$, which is comparable with that of $-40\,^{\circ}\text{C}$ for Au catalyst supported by TiO_2 nanocrystalline P-25. Because of the low drying temperature of 40 °C for the as-synthesized Au catalyst, adsorbed water molecules could remain on the surface of Ti-SBA-15. The observed high activity of the as-synthesized Au catalyst indicated that the adsorbed water did not have a negative effect on the active sites of Au catalysts. Each light-off curve was recorded over 16 h. After the conversion reached 100%, no deactivation was observed. Therefore, this catalyst is highly stable. High-temperature treatment (8% O_2–He, 300 °C, 30 min) dramatically decreased the activity of nanocrystalline TiO_2 supported catalysts, as the light-off curve shifted to high temperature. By contrast, the activity of the Au catalyst supported on Ti-SBA-15 did not change significantly, achieving >50% conversion at $-25\,^{\circ}\text{C}$, which is much lower than that of 25 °C for

nanocrystalline TiO_2 supported catalyst. The high stability of the titania-modified catalyst may be due to the unique surface property of the TiO_2 layer to bind the deposited gold nanoparticles and stabilize the catalytic properties in a high temperature environment.

For comparison, the gold nanoparticles were also deposited on the surface of the unmodified SBA-15 with the DP method. The resulting catalyst showed no activity for CO oxidation even at temperatures as high as 160 °C. The TEM image of the gold-deposited sample (not shown) revealed that a small population of very large gold nanoparticles (>8 nm) aggregated on the external surfaces of SBA-15. Accordingly, the size of the gold nanoparticles is too big to be catalytically active. This observation clearly demonstrated the importance of the TiO_2 surface functionalization for the immobilization and the stabilization of gold nanoparticles.

4. Conclusions

In conclusion, the surface of mesoporous silica SBA-15 was uniformly covered with one layer titanium oxide by a hydrolytic surface sol–gel process. Ultra-small gold nanoparticles (0.8–1 nm) were deposited on the resulting material via a deposition–precipitation technique. X-ray diffraction studies show that deposited gold exists in the form of Au^{3+} and Au^0 in the as-synthesized and reduced catalyst, respectively. The X-ray diffraction analyses also suggested that the metallic Au nanoparticles are more developed along $\langle 1\,1\,1 \rangle$ direction of the fcc lattice forming a raft-type structure. TEM images show that the ultra-small gold nanoparticles are uniformly deposited on the surface of the substrate. The particles show a high catalytic activity for CO oxidation.

References

[1] M. Haruta, Catal. Today 36 (1997) 153.
[2] G.C. Bond, D.T. Thompson, Catal. Rev. Sci. Eng. 41 (1999) 319.

[3] M. Haruta, N. Yamada, T. Kobayashi, S. Iijima, J. Catal. 115 (1989) 301.

[4] D. Thompson, Gold Bull. 31 (1998) 111.

[5] D. Thompson, Gold Bull. 32 (1999) 12.

[6] W.F. Yan, B. Chen, S.M. Mahurin, S. Dai, S.H. Overbury, Chem. Commun. (2004) 1918.

[7] H.L. Lian, M.J. Jia, W.C. Pan, Y. Li, W.X. Zhang, D.Z. Jiang, Catal. Commun. 6 (2005) 47.

[8] M. Besson, A. Kallel, P. Gallezot, R. Zanella, C. Louis, Catal. Commun. 4 (2003) 471.

[9] R.D. Waters, J.J. Weimer, J.E. Smith, Catal. Lett. 30 (1995) 181.

[10] N.S. Patil, B.S. Uphade, D.G. McCulloh, S.K. Bhargava, V.R. Choudhary, Catal. Commun. 5 (2004) 681.

[11] H. Sakurai, M. Haruta, Appl. Catal. A 127 (1995) 93.

[12] S. Arrii, F. Morfin, A.J. Renouprez, J.L. Rousset, J. Am. Chem. Soc. 126 (2004) 1199.

[13] K. Mallick, M.J. Witcomb, M.S. Scurrell, Appl. Catal. A 259 (2004) 163.

[14] Y.Z. Yuan, A.P. Kozlova, K. Asakura, H.L. Wan, K. Tsai, Y. Iwasawa, J. Catal. 170 (1997) 191.

[15] A.I. Kozlov, A.P. Kozlova, K. Asakura, Y. Matsui, T. Kogure, T. Shido, Y. Iwasawa, J. Catal. 196 (2000) 56.

[16] J.D. Grunwaldt, C. Kiener, C. Wogerbauer, A. Baiker, J. Catal. 181 (1999) 223.

[17] T. Kobayashi, M. Haruta, S. Tsubota, H. Sano, B. Delmon, Sens. Actuat B 1 (1990) 222.

[18] S. Tsubota, M. Haruta, T. Kobayashi, A. Ueda, Y. Nakahara, Stud. Surf. Sci. Catal. 63 (1991) 695.

[19] M. Okumura, K. Tanaka, A. Ueda, M. Haruta, Solid State Ionics 95 (1997) 143.

[20] M. Okumura, S. Tsubota, M. Iwamoto, M. Haruta, Chem. Lett. (1998) 315.

[21] M. Haruta, Cattech 6 (2002) 102.

[22] I. Ichinose, H. Senzu, T. Kunitake, Chem. Mater. 9 (1997) 1296.

[23] J.G. Huang, T. Kunitake, J. Am. Chem. Soc. 125 (2003) 11834.

[24] J.H. He, I. Ichinose, T. Kunitake, A. Nakao, Y. Shiraishi, N. Toshima, J. Am. Chem. Soc. 125 (2003) 11034.

[25] M. Leskela, M. Ritala, Angew. Chem., Int. Ed. 42 (2003) 5548.

[26] T. Yasuda, R. Kuse, K. Iwamoto, K. Tominaga, J.W. Park, Chem. Mater. 15 (2003) 4157.

[27] J.W. Elam, D. Routkevich, P.P. Mardilovich, S.M. George, Chem. Mater. 15 (2003) 3507.

[28] W.F. Yan, B. Chen, S.M. Mahurin, E.W. Hagaman, S. Dai, S.H. Overbury, J. Phys. Chem. B 108 (2004) 2793.

[29] S.J. Lee, A. Gavriilidis, J. Catal. 206 (2002) 305.

[30] G. Cagliotti, A. Paoletti, F.P. Ricci, Nucl. Instrum. 3 (1958) 223.

[31] W. Kraus, G. Nolze, PowderCell – a program for structure visualization, powder pattern calculation and profile fitting. Available from: <http://www.ccp14.ac.uk/>.

[32] ICSD Collection Code 44362.

[33] ICSD Collection Code 64923.

[34] F. Cotton, G. Wilkinson, Advanced Inorganic Chemistry, third ed., Wiley, New York, 1972.

[35] C. Suryanarayana, M.G. Norton, X-ray Diffraction, Plenum Press, New York, 1998.